CHEMISTRY OF
MATERIALS
Article

Chem. Mater. XXXX, *XXX*, 000–000 A
DOI:10.1021/cm9030599

Size Controlled Synthesis of Germanium Nanocrystals by Hydride Reducing Agents and Their Biological Applications

Sujay Prabakar,[†] Amane Shiohara,[†] Sanshiro Hanada,[‡] Kouki Fujioka,[‡] Kenji Yamamoto,[‡] and Richard D. Tilley*,[†]

[†]*School of Chemical and Physical Sciences and MacDiarmid Institute of Advanced Materials and Nanotechnology, Victoria University of Wellington, New Zealand and* [‡]*International Clinical Research Centre, Research Institute, International Medical Centre of Japan*

Received October 2, 2009. Revised Manuscript Received October 27, 2009

Germanium nanocrystals were synthesized by the hydride reduction of germanium tetrachloride ($GeCl_4$) in inverse micelles using hydride reducing agents including lithium aluminum hydride ($LiAlH_4$), lithium triethyl borohydride ($Li(C_2H_5)_3BH$), lithium borohydride ($LiBH_4$), and sodium borohydride ($NaBH_4$). Monodisperse Ge nanocrystals with average sizes ranging from 4.0 to 5.5 nm were produced using a simple room temperature technique. The nanocrystals were capped using allylamine. The nanocrystals displayed strong blue luminescence, and their application as optical probes is demonstrated by the imaging of HepG2 cells. Transmission electron microscopy (TEM), selected area electron diffraction (SAED), energy dispersive X-ray spectroscopy (EDX), and fluorescence spectroscopy were used to characterize the nanocrystals. The cytotoxicity of the nanocrystals is also reported, and the germanium quantum dots were found to be relatively nontoxic.

Introduction

The synthesis of nanocrystalline semiconductor materials with controlled sizes and biological compatibility are important in current material science research and has attracted a lot of interest in recent years.[1,2] Biological applications such as biosensing and cell imaging requires tuning the opto-electronic and surface properties, therefore making it essential to produce semiconductor nanocrystals with narrow size distributions in the 3−8 nm size region that are stable and water-soluble.[3,4] In recent years, a need for versatile and reliable imaging agents has stemmed from the fact that standard fluorescent labels such as organic dyes have been reported to be limiting, due to factors such as signal intensity strength, short lifetimes, and narrow excitation ranges.[5] Semiconductor nanocrystals have improved optical qualities desirable for biological applications compared to organic dyes, making their controlled synthesis and surface functionalization a very active area of research.[6−10]

Quantum dots are becoming popular as replacements for fluorescent dyes in biological fluorescence imaging because of their superior resistance to photobleaching. To date, considerable emphasis has been placed on using CdSe based quantum dots as biological chromophores, since they emit light that can be tuned throughout the visible spectrum.[11] However, concerns have been raised about the toxicological issue of quantum dots in living systems. Quantum dot toxicity can stem from two sources: (i) the quantum dot core and (ii) the capping molecule. A seminal study by Derfus et al. showed that quantum dots with a CdSe core and without a ZnS shell, after exposure to UV light, were toxic to liver cells.[12] The relatively low toxicity, and facile synthesis of photoluminescent germanium quantum dots make them ideal for biological fluorescence imaging and should eliminate any potential toxicology problems of quantum dots that might arise from having a CdSe core.[13−15]

Germanium nanocrystals are expected to exhibit photoluminescence in the visible region and quantum confinement effects due to the relatively large excitonic

*Corresponding author. E-mail: richard.tilley@vuw.ac.nz.

(1) Alivisatos, A. P. *J. Phys. Chem.* **1996**, *100*, 13226–13239.
(2) Heath, J.; Shiang, J.; Alivisatos, A. P. *J. Chem. Phys.* **1994**, *101*, 1607–1615.
(3) Tilley, R. D.; Yamamoto, K. *Adv. Mater.* **2006**, *18*(15), 2053–2056.
(4) Warner, J. H.; Tilley, R. D. *Nanotechnology* **2006**, *17*(15), 3745–3749.
(5) Walling, M. A.; Novak, J. A.; Shepard, J. R. *Int. J. Mol. Sci.* **2009**, *10*(2), 441–491.
(6) Alivisatos, A. P. *Nat. Biotechnol.* **2004**, *22*, 47–52.
(7) Michalet, X. F.; Pinaud, L. A.; Bentolila, J. M.; Tsay, S.; Doose, J.; Li, J.; Sundaresan, G.; Wu, A. M.; Gambhir, S. S.; Weiss, S. *Science* **2005**, *307*, 538–544.
(8) Bruchez, M. B.; Moronne, M.; Weiss, S.; Alivisatos, A. P. *Science* **1998**, *281*, 2013–2016.
(9) Wu, X.; Liu, H.; Liu, J.; Haley, K. N.; Treadway, L. A.; Larson, J. P.; Ge, N.; Peale, F.; Bruchez, M. P. *Nat. Biotechnol.* **2003**, *21*, 41–46.
(10) Dahan, M.; Levi, S.; Luccardini, C.; Rostaing, P.; Riveau, B.; Triller, B. *Science* **2003**, *302*, 442–445.
(11) Al-Salim, N.; Young, A. G.; Tilley, R. D.; McQuillan, A. J.; Xia, J. *Chem. Mater.* **2007**, *19*, 5185–5193.
(12) Derfus, A. M.; Chan, W. C.; Bhatia, S. N. *Nano Lett.* **2004**, *4*, 11.
(13) Chang, E.; Thekkek, Nadhi.; Yu, W. W.; Colvin, L. V.; Drezek, R. *Small* **2006**, *12*, 1412–1417.
(14) Kirchner, C.; Liedl, T.; Kudera, S.; Pellegrino, T.; Javier, A. M.; Gaub, H. E.; Stoelzle, S.; Fertig, N.; Parak, W. J. *Nano Lett.* **2005**, *5*, 331.
(15) Chan, W.-H.; Shiao, N.-H. *Acta Pharmacol. Sin.* **2008**, *29*, 259–266.

Bohr radius (R_b = 11.5 nm) and have been proposed for use in different applications because of their unique optical properties.[16,17] However, reports on germanium nanocrystals as biological tools/labels are few. For example, Boyle et al. reported the synthesis of ~3−5 nm phospholipid-encapsulated water-soluble germanium nanocrystals that were used as biomarkers for cell signaling in RBL-2H3 cells in vitro.[18] For germanium nanocrystals to be used in biological applications, photoluminescence quantum yield in the visible region and water solubility are vital. Thus the development of synthetic methods for producing germanium nanocrystals with controlled sizes and modified surfaces, with low toxicity, is important for the biological applications of germanium nanocrystals.

Germanium nanocrystals have previously been produced using different methods.[19−24] Veinot et al. produced alkyl-surface functionalized germanium nanocrystals via metal hydride reduction of nonpolar solutions of CTAB and GeI_4 at room temperature.[19] Kauzlarich et al. investigated the synthesis of germanium nanoparticles by the sodium naphthalide reduction of $GeCl_4$ varying reactions conditions.[20] Korgel et al. formed high yields of Ge nanocrystals by the reduction of GeI_4 by $LiAlH_4$ in high boiling point solvents.[21] Supercritical solvents have also been used to synthesize reasonable yields of germanium nanocrystals.[22−24]

The size controlled syntheses of monodisperse germanium nanocrystals using colloidal routes that involve high reaction temperature are well established. However, less progress has been made in the low temperature synthesis of Ge nanocrystals mainly because of its covalency.[25] The high temperature solution synthesis method to form Ge nanocrystals typically requires temperatures ranging from 270 °C to as high as 429 °C.[2,26] Such techniques, while useful in producing highly crystalline nanocrystals, are challenging, because of the instability of organic moieties such as solvents and capping agents at elevated temperatures which can generate hard to remove impurities. Additionally, interpretation of fluorescence data becomes difficult as reactive free radicals from the decomposition of organic solvents produce luminescence.[27]

Thus, while solution methods involving high temperatures are well established for germanium nanocrystals, room temperature syntheses that produce water-soluble, monodisperse germanium nanocrystals for cell imaging have not, to the best of our knowledge, been previously reported.

Here we show a simple method for the size controlled synthesis of photoluminescent germanium nanocrystals using reverse micelles and hydride reducing agents at room temperature. The hydride terminated nanocrystals were then surface stabilized and made water-soluble by capping with allylamine. The method reported here utilizes hydride reducing agents of different strengths to control nanoparticle size and produce hydrogen-terminated surfaces that could be used to react with compounds containing a C=C bond to produce different surface functionalities through the formation of a Ge−C surface bond.

The difference in reactivity of the different hydride reducing agents is used to control the sizes of nanocrystals formed in the reaction. Through controlling the size of the germanium nanocrystals, the photoluminescence properties of the quantum dots could be tuned.

Experimental Section

Synthesis and Purification. All of the chemicals used in this experiment were of analytical grade. In a typical synthesis, 50 mL of anhydrous hexane (Aldrich, ≥99%) was added to a 3-necked flask attached to a Schlenk line and purged with nitrogen. A total of 0.026 g of pentaethylene glycol monododecyl ether ($C_{12}E_5$), a nonionic surfactant (Nikko Chemicals Co, >98%), and 100 μL of $GeCl_4$ (Aldrich, ≥99.0%) was removed from the glovebox in an airtight syringe and injected into the reaction flask. Germanium nanocrystals were then formed by adding a stoichiometric amount (1:4, $GeCl_4$:reductant) of a solution of either $LiAlH_4$ (1.0 M in THF), $Li(Et)_3BH$ (1.0 M in THF), $LiBH_4$ (2.0 M in THF), or $NaBH_4$ (2.0 M in triethylene glycol dimethyl ether) as reducing agent and were all purchased from Aldrich Chemicals. After the above mixture was left to react for 2 h, the surface of the nanocrystals is terminated with hydrogen. A total of 40 μL of H_2PtCl_6 (99.995%, Aldrich) in anhydrous isopropanol (99.5%, Aldrich) as catalyst and 2 mL of allylamine (≥99%, Aldrich) were added to modify the surface germanium−hydrogen bonds, thus rendering the nanocrystals water-soluble.

The water-soluble Ge nanocrystals were purified by first removing the solvent by rotary evaporation to produce a yellow viscous oil. A total of 50 mL of distilled water was then added to the flask, in which the nanocrystals but not the $C_{12}E_5$ dissolved, which is subsequently removed by filtration. After sonication for 5 min the solution was further filtered using a Millipore 0.45 μm membrane filter. The filtrate was concentrated to about 1 mL and then purified down a Sephadex gel LH-20 (bead size 25−100 μm) column (φ = 1 cm). The luminescent fraction was then collected and concentrated down to 1 mL to give a solution of water-soluble germanium nanocrystals.

Characterization. Transmission electron microscopy images and electron diffraction patterns were acquired digitally with a JEOL 2010 operated at an accelerating voltage of 200 KeV. EDS data were acquired on a JEOL 2010 equipped with an Oxford Inca EDS detector. Photoluminescence spectra were obtained

(16) Wilcoxon, J. P.; Provencio, P. P.; Samara, G. A. *Phys. Rev. B* **2001**, *64*, 035417.
(17) Wilcoxon, J. P.; Provencio, P. P.; Samara, G. A. *Phys. Rev. B* **1999**, *60*, 2704.
(18) Lambert, T. N.; Andrews, N. L.; Gerung, H.; Boyle, T. J.; Oliver, J. M.; Wilson, B. S.; Han, S. M. *Small* **2007**, *3*(4), 691–699.
(19) Fok, E.; Shih, M.; Meldrum, A.; Veinot, J. C. *Chem. Commun.* **2004**, 386–387.
(20) Chiu, H. W.; Kauzlarich, S. M. *Chem. Mater.* **2006**, *18*, 1023–1028.
(21) Lu, X.; Korgel, B. A.; Johnston, K. P. *Chem. Mater.* **2005**, *17*, 6479–6485.
(22) Lu, X.; Ziegler, K. J.; Ghezelbash, A.; Johnston, K. P.; Korgel, B. A. *Nano Lett.* **2004**, *4*, 969.
(23) Myung, N.; Lu, X.; Johnston, K. P.; Bard, A. J. *Nano Lett.* **2004**, *4*, 183.
(24) Lu, X.; Korgel, B. A.; Johnston, K. P. *Nanotechnology* **2005**, *16*, S389.
(25) Wu, H. P.; Liu, J. F.; Wang, Y. W.; Zeng, Y. W.; Wu, J. J. *Mater. Lett.* **2006**, *60*, 986.
(26) Zaitseva, N.; Dai, Z. R.; Grant, C. D.; Harper, J.; Saw, C. *Chem. Mater.* **2007**, *19*, 5174–5178.
(27) Gerion, D.; Zaitseva, N.; Saw, C.; Casula, M. F.; Fakra, S.; Buuren, T. V.; Galli, G. *Nano Lett.* **2004**, *4*(4), 597–602.

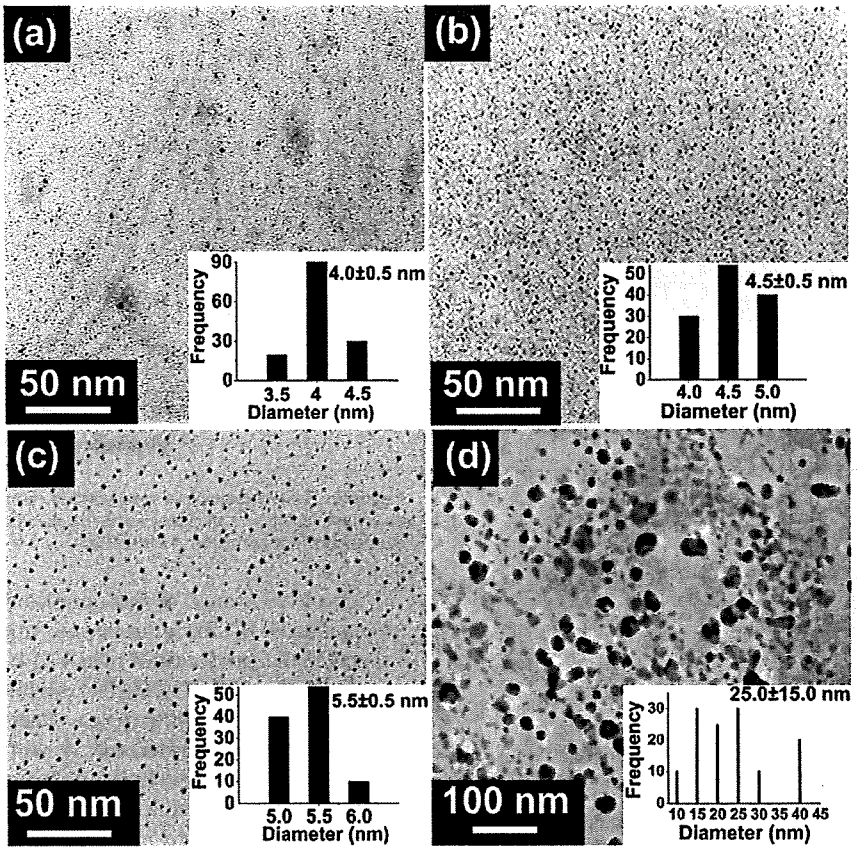

Figure 1. TEM images of Ge nanocrystals obtained from reduction by (a) $LiAlH_4$ and (b) $Li(C_2H_5)_3$, (c) $LiBH_4$, and (d) $NaBH_4$.

using a J-Y Fluorolog fluorescence spectrometer, with a slit width of 5 nm in both emission and excitation.

Incorporation of Ge Nanocrystals into HepG2 Cells. HepG2 cells were used with assays conducted at 1.0 μg/mL for 6 h of incubation. The germanium nanocrystals were excited with a mercury lamp, and the images were captured on a cooled charge-coupled device (CCD), mounted on a fluorescent microscope IX-81 (Olympus) with an excitation filter 330−380 nm.

Results and Discussion

It has been previously shown that by using reducing agents with different reactivities, the size of the resulting nanocrystals can be controlled.[20] To compare the effect of reductants in our reaction, four experiments were conducted. The first used $LiAlH_4$ as reductant, primarily because of its powerful reducing capability and also since it has been previously shown to produce nanocrystals of narrow size distribution.[28] Additionally $Li(C_2H_5)_3BH$ (superhydride), $LiBH_4$, and $NaBH_4$ were used with the strength of the reducing agents decreasing along this list with $LiAlH_4$ being the strongest and $NaBH_4$ the weakest. In this study, all other experimental variables were kept constant, and the samples were reacted for 3 h at room temperature, with the reducing agents added in one swift injection.

Figure 1 shows low-resolution transmission electron microscope (TEM) images of a number of allylamine capped germanium nanocrystals. The images illustrate that the selective use of the hydride reducing agents can control the size of the resulting Ge nanocrystals.

Figure 1a is low resolution TEM image of germanium nanocrystals obtained from the reduction using $LiAlH_4$. The nanocrystals had average sizes of 4.0 with a range of sizes of ±0.5 nm (based on 300 nanoparticles) and are predominantly spherical. Figure 1b,c are low resolution TEM images of germanium nanocrystals obtained from the reduction using $Li(Et)_3BH$ and $LiBH_4$, respectively. The nanoparticles were again found to be predominantly spherical and relatively monodisperse with average sizes of 4.5 nm and a range of sizes of ±0.5 nm (based on 500 particles) and 5.5 nm and a range of sizes of ±0.5 nm (based on 250 particles), respectively. Figure 1d is a low resolution TEM image of germanium nanocrystals obtained from the reduction using $NaBH_4$. The nanoparticles were found to be larger in size and were irregularly shaped nanocrystals with an average size of 25.0 ± 15.0 nm (based on 300 particles).

The reaction with $LiAlH_4$ produced the smallest nanocrystals (4.0 ± 0.5 nm) as shown in Figure 1a. The reaction using $LiAlH_4$ as the reducing agent proceeds vigorously and quickly due to the strong reducing capability of $LiAlH_4$. As a result of this rapid reduction there is a quick depletion of monomers with few monomers remaining for further growth of the nanocrystals, hence, the small particle size. A similar trend is observed for the

(28) Tilley, R. D.; Warner, J. H.; Yamamoto, K.; Matsui, I.; Fujimori, H. *Chem. Commun.* **2005**, *14*, 1836.

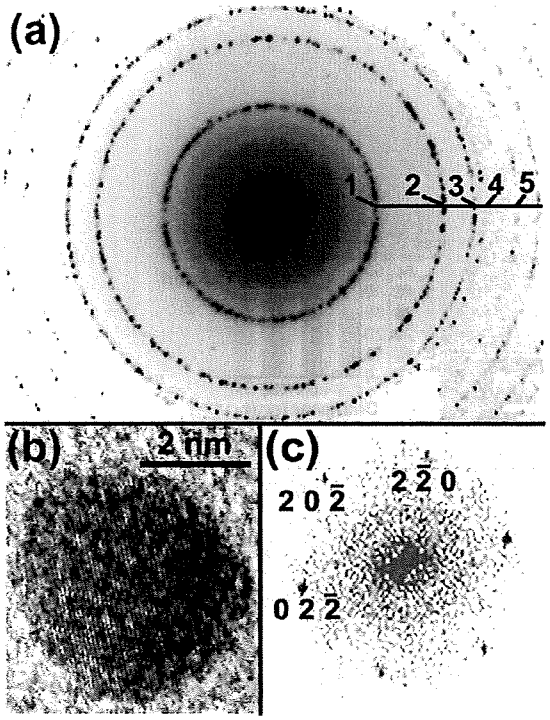

Figure 2. (a) Selected-area electron diffraction pattern (SAED) for Ge nanocrystals obtained from the hydride reduction of $GeCl_4$, rings matched the diamond germanium planes: Ring 1 = (111), 2 = (220), 3 = (311), 4 = (400), and 5 = (331). (b) high-resolution TEM image of an amine-terminated Ge nanocrystal synthesized using $LiAlH_4$ as reductant, viewed down the [111] direction (c) corresponding fast Fourier transform (FFT) of the image.

reduction by $Li(C_2H_5)BH$ and $LiBH_4$, but due to their lower reactivity compared to $LiAlH_4$, slightly larger nanoparticle sizes are obtained. $NaBH_4$ is a weak reducing agent, and when injected into the solution there is less monomer depletion in the nucleation burst leaving considerable unreacted monomer that contributes to nanoparticle growth, causing the formation of nanoparticles of large size.

The ability to control particle size in group IV nanocrystals using reducing agents is uncommon and to the best our knowledge not reported for systems involving hydride reducing agents and inverse micelles. Of particular significance is the ability to control nanoparticle size in the quantum confinement size regime.

Confirmation of the crystal structure of the germanium nanocrystals was obtained from selected-area electron diffraction (SAED) and is shown in Figure 2a. The SAED rings matched well with the diamond crystal structure adopted by germanium. Figure 2b is a high-resolution TEM image (HRTEM) of a 4 nm germanium nanocrystal obtained from the reaction using $LiAlH_4$ as reductant. The nanocrystal is highly crystalline with the lattice fringes clearly observable. The fast Fourier transform of the HRTEM image in Figure 2c exhibits the characteristic pattern of the diamond germanium crystal structure, viewed down the [111] direction. Crystalline nanocrystals of germanium such as these were obtained for all hydride reducing agents.

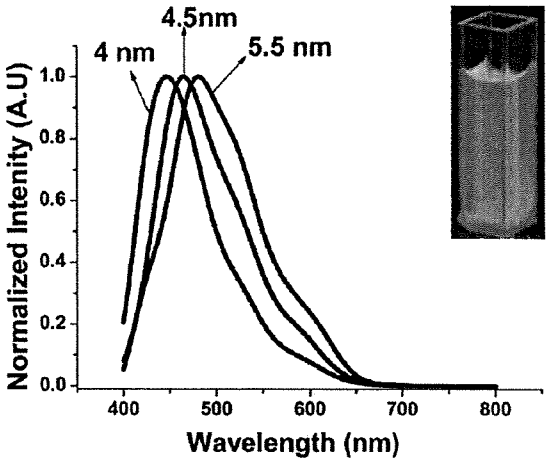

Figure 3. Photoluminescence spectra of amine-terminated Ge nanocrystals excited at 400 nm. The inset shows the fluorescence of the germanium nanocrystals excited under a UV lamp.

Figure 3 shows the 400 nm photoluminescence spectra (normalized) of an aqueous solution of allylamine-capped Ge nanocrystals of sizes 4.0, 4.5, and 5.5 nm made using $LiAlH_4$, $Li(C_2H_5)_3BH$ (superhydride), and $LiBH_4$, respectively. Emission across a relatively narrow region of 420−480 nm is observed with full width maxima (fwhm) of 70−80 nm indicating the monodisperse nature of the Ge nanocrystals. The PL peaks between 420 to 480 nm are similar to previous reports of Ge nanocrystals.[11,29] Quantum yield measurements based on the comparative method of Williams and co-workers relative to the standard 9,10- diphenylanthracene in cyclohexane indicated the germanium nanocrystals had a quantum yield of approximately 11%.[30−32]

As expected, no photoluminescence from direct band gap transitions was detected from the nanocrystals of average size 25 nm, which were too big to be in the quantum confinement regime. These results are important as they illustrate the ability to control nanoparticle size in the quantum confinement regime leading to the Ge nanocrystals exhibiting tunable photoluminescence in the visible wavelength region via direct band gap transitions.[33−36]

One application of germanium nanocrystals is as imaging agents for cell biology, and this application is demonstrated with HepG2 cells. Figure 4 shows the overlay of the transmission and fluorescence image obtained from HepG2 cells with Ge nanocrystals transfected into

(29) Gerung, H.; Bunge, S. D.; Boyle, T. J.; Brinker, C. J.; Han, S. M. *Chem. Commun.* **2005**, 1914−1916.
(30) Williams, A. T. R.; Winfield, S. A.; Miller, J. N. *Analyst* **1983**, *108*, 1067.
(31) Hamai, S.; Hirayama, F. *J. Phys. Chem.* **1983**, *87*, 83.
(32) Warner, J. H.; Hoshino, A.; Yamamoto, K.; Tilley, R. D. *Angew Chem., Int. Ed.* **2005**, *44*, 4550.
(33) Warner, J. H.; Rubinsztein-Dunlop, H.; Tilley, R. D. *J. Phys. Chem B.* **2005**, *109*, 19064−19067.
(34) Taylor, B. R.; Kauzlarich, S. M.; Delgado, G. R.; Lee, H. W. H. *Chem. Mater.* **1999**, *11*, 2493.
(35) Henderson, E. J.; Hessel, C. M.; Veinot, J. G. C. *J. Am. Chem. Soc.* **2008**, *130*, 3624.
(36) Ma, X.; Wu, F.; Kauzlarich, S. M. *J. Solid State Chem.* **2008**, *181*, 1628.

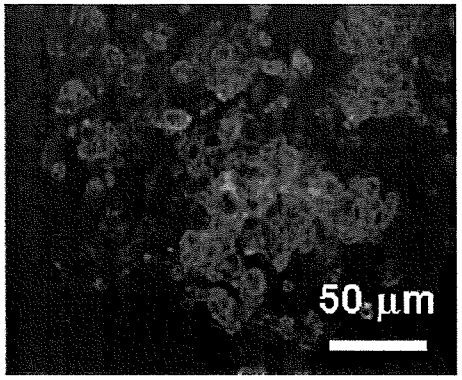

Figure 4. Overlay of the transmission and fluorescence microscopy image of HepG2 cells with germanium nanocrystals transfected inside the cytosol.

the cytosol. The blue fluorescence from direct-bandgap emission from the Ge nanocrystals in the HepG2 cells illustrates the use of hydrophilic germanium nanocrystals as biological fluorescence imaging agents.

To use germanium nanocrystals in biological imaging the effect on cell activity should be known. Mitochondrial activity in 0−1000 μg/mL of germanium nanocrystals was investigated with HePG2 cells as a carcinoma cell line. From the histogram in Figure 5, the 50%-inhibitory toxicity concentration (TC50) with HePG2 cells was calculated and found to be 100 μg/mL. This indicates that germanium nanocrystals could be used at concentrations of 100 μg/mL and have relatively low toxicity. A TC50 of 100 μg/mL is lower than that reported by Fujioka and co-workers for CdSe quantum dots exposed to UV light with HeLa cells.[37] This present study can provide the basis for future advances on the cytotoxicity of germanium nanoparticles.

(37) Fujioka, K.; Hiruoka, M.; Sato, K.; Manabe, N.; Miyasaka, R.; Hanada, S.; Hoshino, A.; Tilley, R. D.; Manome, Y.; Hirakuri, K.; Yamamoto, K. *Nanotechnology* **2008**, *19*, 415102.

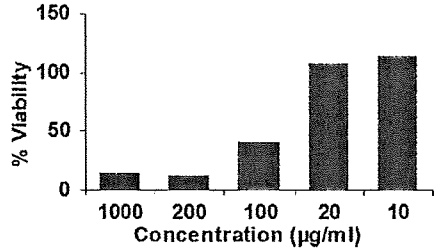

Figure 5. Toxicity studies: mitochondrial activity of HePG2 cells cultured with germanium nanocrystals.

Conclusions

In conclusion germanium nanocrystals with narrow size distributions were synthesized in reverse micelles and powerful reducing agents at room temperature and pressure. By using the difference in reactivity of the reducing agents, size control of the quantum dot was achieved. It was observed that by using $LiAlH_4$, the strongest reductant, small nanoparticles could be obtained, and by using weaker reductants such as $NaBH_4$, larger nanoparticles were obtained. The surface of the germanium nanocrystals were made water-soluble by capping with allylamine. The germanium nanocrystals were purified by column chromatography. The germanium nanocrystals dispersed in aqueous solvents displayed strong photoluminescence in the blue region of the visible spectrum. The amine functionalized germanium nanocrystals were used for the imaging of HePG2 cells and were shown to be relatively nontoxic. The optical properties, purity, and cell compatibility of the germanium nanocrystals reported here make them excellent candidates for future biological optical probes.

Acknowledgment. R.D.T. thanks the Macdiarmid Institute for funding. S.P., A.S., and R.D.T. thank FRST for funding through Grant HOF VICX0601.

Peptide Science 2008: M. Nomizu (Ed.)
The Japanese Peptide Society (2009)

Nano-Particle Materials Prepared From a Synthetic Antigenic Sequence of *Plasmodium falciparum* Enolase

Hiroyuki Oku, Keiichi Yamada, Kyoko Kobayashi, Ryoichi Katakai, Muhammad Ashfaq[1], Hirofumi Hanaoka, Yasuhiko Iida[2], Keigo Endo[3], Shin Hasegawa, Yasunari Maekawa[4], Kazuhiko Yano, Shigeyuki Kano[5], Mamoru Suzuki[6]

[1]Department of Chemistry& Chemical Biology, Gunma University, Kiryu, Gunma 376-8515, Japan, [2]Departments of Bioimaging Information Analysis and Diagnostic Radiology and [3]Nuclear Medicine, Gunma University Graduate School of Medicine, Maebashi, Gunma 371-8511, Japan, [4] Takasaki Advanced Radiation Research Institute, Japan Atomic Energy Agencytomic Energy, Takasaki, Gunma 370-1292, Japan, [5]Research Institute, International Medical Center of Japan, Shinjyuku, Tokyo 162-8655, Japan, [6]Gunma University, Maebashi, Gunma 371-8510, Japan.
e-mail: oku@chem-bio.gunma-u.ac.jp

Malaria is the major cause of mortality and morbidity in the tropical and subtropical regions in the world. Our previous studies have shown that a series of partial peptides of a Plasmodium falciparum enolase have antigenic reactivity against patients' sera. In this paper, we wish to report nano-encapsulation of a synthetic antigen into bioabsorbable polymer particles and their releasing studies in vitro and in vivo.

Keywords: *Plasmodium falciparum, enolase, malaria, peptide, antigen, nanosphere, fluorescence spectroscopy, in vivo imaging.*

Introduction

The newest survey, *World Malaria Report 2008* [1] has described that half of the world's population is at risk of malaria, and an estimated 247 million cases led to nearly 881,000 deaths in 2006 especially caused by falciparum malaria caused by the infection one of in 2006. In Japan, although indigenous malaria was eradicted in 1961, an increasing number of grobal travel has resulted 100-170 cases of imported malaria per year [2].

We have studied a glycolytic enzyme, enolase [3] from *Plasmodium falciparum* (*P.f.*), which is the most lethal among four malarial parasites caused human infection. In 1990, an antigen toward *P.f.* enolase was found in patients'

sera based on the field studies by Kano and Suzuki [4]. This is a probable evidence to support an epidemiological view of which residents in an endemic area are often immune to malaria. To prove this finding, we have started synthetic studies of partial peptides based on the amino acid sequence of *P.f.* enolase, and successfully found similar antigenic property [5]. Among several sequences, we have especially focused on a sequence Ala^{256}-Asp^{277} (AD22, Figures 1c) by using solid and solution phase methods in our laboratory [6]. Our reaserch goal is to make a vaccination materials to realize the immunity condition in endemic area.

For the development of effective malaria control methods, micro- and nano-particles made of polymers and inorganic materials have been intensively investigated for *in vivo* vaccine formulation systems [7] and *in vitro* diagnostic devices [8]. In this paper, we wish to report nano-encapsulation and slow releasing studies *in vitro* and *in vivo* of the synthetic enolase antigen in bioabsorbable polymer particles.

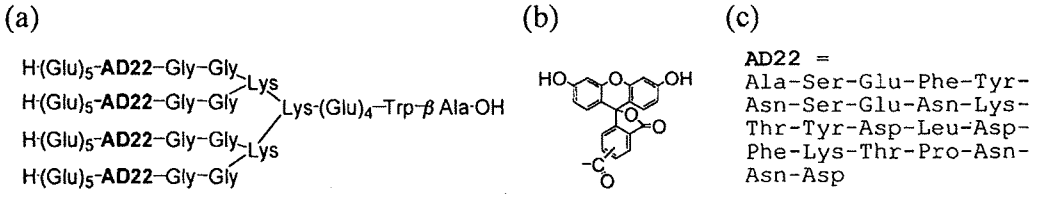

Figure 1. (a) Antigenic peptide (1) and (b) a fluorescent label, 5(6)-carboxy-fluorescein, used in this study. (c) A potential antigenic sequence, Ala^{256}-Asp^{277} (AD22) in P.f. enolase is incorporated in this peptide.

Results and Discussion

The peptide antigen **1** was constructed by solid-phase synthesis using Fmoc-amino acids bearing benzyl-type protecting groups on the side chain functional groups. For amino acid analysis of **1**, acid hydrolysis was carried out with a 4 M CH_3SO_3H aqueous solution at 110°C for 24 h. The observed (calculated) composition of amino acids are follows: Asp and Asn, 28.8 (28); Glu, 33.1 (32); Ser 7.9 (8); Thr, 7.7 (8); β-Ala, 1.9 (1); Ala, 3.9 (4); Pro, 4.2 (4); Tyr, 7.8 (8); Leu, 4.0 (4); Phe, 8.0 (8); Trp 1.4 (1); Lys 23.6 (22). **1** was also labeled with 5(6)-carboxyfluorescein (CF) and used for the nano-encapsulation in poly(lactic acid-*co*-glycolytic acid) (PLGA).

PLGA nanospheres were formulated using an oil/water emulsion technique. For example, 2 mg of CF-**1** in 2 mL of acetic acid was emulsified in 7.0 mL CH2Cl2 containing 375 mg PLGA (75:25 for lactic and glycolytic acid, mw~20,000) using a probe type ultrasonic homogenizer. The resulted primary emulsion was added into 180 mL of 0.5% poly(vinylalcohol) and was further homogenized to form the secondary emulsion. The secondary emulsion was continued stirring for 5h to complete hardning. The produced microspheres were then collected by centrifugation (2,000g). Particle size was determined with a scanning electron microscope, presented a distribution between 0.3 and 1.5 mm as shown in Figure 2a.

Fluorescence intensity has shown the loading of CF-**1** was determined as 4.0

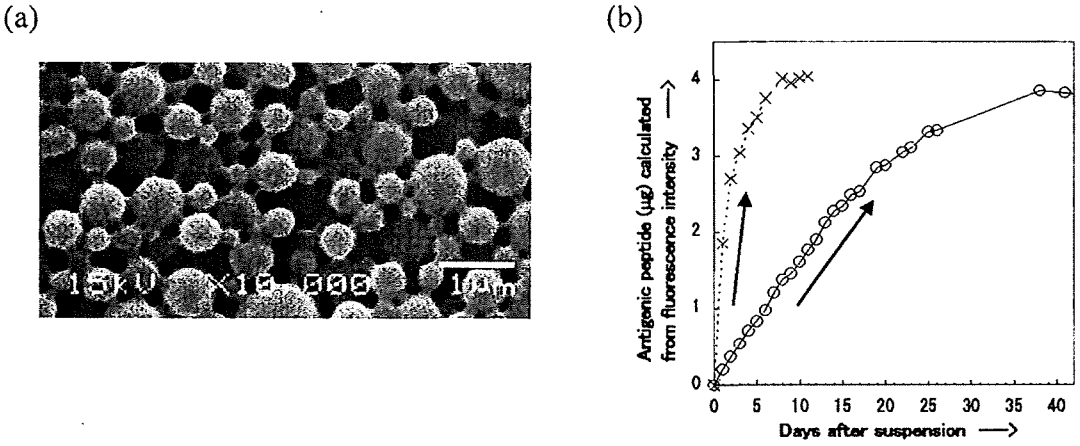

Figure 2. (a) Scanning electron micrograph of antigen loaded microspheres. (b) Cumulative in vitro release profiles of CF-1 from nano-spheres (-O-) in 0.2% SDS containing PBS at 37°C. As a comparison, the fluorescence intensity changes were plotted for the suspension of CF-1 (-x-). From this profile, CF-1 dissolves slowly in SDS-PBS solvent due to difficult solubility of the antigenic sequence. Conditions: fluorescent spectrophotometer (JASCO FP6200); excitation at 490 nm; detection at 500-650 nm; slit width 5 nm.

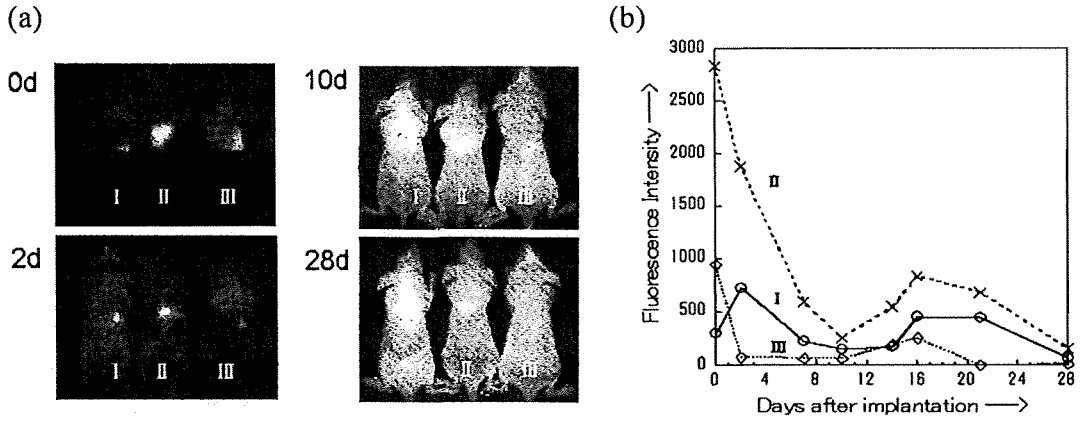

Figure 3. (a) Fluorescence images after subcutaneous implantation of biodegradable nano-particles containing a carboxy-fluorescein labeled synthetic peptide. Conditions: fluorescence imager (CRi Maestro FL500); excitation 445-490 nm (band-path filtered); detection 500-720 nm (spectral images taken every 10 nm). (b) Fluorescence intensity changes after implantation were plotted from the resolved images of fluorescein spectrum.

μg in 1.0 mg of nanospheres. The release profile of the antigen CF-1 from the particles evidenced nearly zero-order kinetics (Figure 2b). Therefore, with this

preparation method, the nanospheres did not show first release ("initial burst") property.

Understanding the *in vivo* behavior of polymeric nano-spheres is crucial for the successful application of this antigen delivery system. Therefore, 1.0 mg nanospheres containing fluorescein-labeled antigen (4.0 μg) were suspended in physiological saline and implanted subcutaneously in each nude mouse. As shown in Figure 3b, obtained images of experimental mice showed that the fluorescence intensity gradually decreased to minimum level until 12 days. Interestingly, the intensity was increasing at 12~16 days and then decreasing again at 16~28 days. This first intensity change is attributable to the degradation or phagocytosis. The second intensity changes are due to the fluorescein uptake by adipocytes which is actually observed in tissue sections. This result shows that antigen containing nanospheres are a viable candidate for long-acting nano-particular protein delivery.

This research is supported by a reserch grant from Japan Science and Technology Agency (for H.O., K.Y., and S.K.), by a Medical Techniques Promotion Research from the Ministry of Health, Labor and Welfare of Japan (for S.K.), and by a post doctral fellowship from Higher Education Commission, Pakistan (for M.A.).

References

1. "*World Malaria Report 2008*", World Health Organization (2008).
2. (a) Kano, S. and Kimura, M. (2004) *Acta. Trop.*, **89**, 271-278. (b) Miura, T., Kimura, M., Koibuchi, T., Endo, T., Nakamura, H., Odawara, T., Wataya, Y., Nakamura, T., and Iwamoto, (2005) *Am. J. Trop. Med. Hyg.*, **73**, 599-603.
3. (a) Read, M., Hicks, K. E., Sims, P. F., Hyde, J. E. (1994) *Eur J Biochem.* **220**, 513-520. (b) Sato K, Kano S, Matsumoto Y, Glanarongran R, Krudsood S, Looareesuwan S, Aikawa M, Suzuki M. (2000) *J. Trop. Med. Public Health.* **31** Suppl 1, 79-84. (c) Pal-Bhowmick, I., Mehta, M., Coppens, I., Sharma, S., Jarori, G. K. (2007) Infect Immun. **75**, 5500-5508.
4. (a) Kano, S. (1990) *Japan. J. Trop. Med. Hyg.*, **18**, 317-324. (b) Norazumi, M. K., and Kano, S. (1996) *Japan. J. Trop. Med. Hyg.*, **24**, 223-229.
5. (a) Karasawa, M., Kobayashi, K., Oku, H., Sato, K., Kano, S., Suzuki, M., Katakai, R. (2000) *Peptide Science 1999, 295-298.* (b) Ishiguro, T., Oku, H., Yamada, K., Sato, K, Kano, S., Suzuki, M., Katakai, R. (2001) *Peptide Science 2000*, 293-296.
6. (a) Omi, K., Kuriyama, K., Yamada, K., Oku, H., Kano, K., Sato, K., Suzuki, M., Katakai, R. (2005) *Peptide Science 2004*, 637-640. (b) Yamamoto, J., Omi, K., Yamada, K., Oku, H., Kano, S., Sato, K., Suzuki, M., Katakai, R. (2006) *Peptide Scienece 2006*, 35-36.
7. (a) Carcaboso, A. M., Hernández, R. M., Igartua, M., Rosas, J. E., Patarroyo, M. E., Pedraz, J. L..Potent, (2004) *Vaccine*, **22**, 1423-1432. (b) Rosas, J. E., Hernández, R. M., Gascón, A. R., Igartua, M., Guzman, F., Patarroyo, M. E., Pedraz J. L. (2001) *Vaccine*, **19**, 4445-4451.
8. (a) Safranj, A., Kano, S., Yoshida, M., Omichi, H., Katakai, R., and Suzuki, M. (1995) *Jpn. J. Parasitol.*, **44**, 170–173. (b) Garcia, M., Kirimoama, S., Marlborough, D., Leafasia, J., Rieckmann, K. H., (1996) *Lancet*, **347**, 1549.

GASTROENTEROLOGY 2009;136:912-923

TWEAK/Fn14 Pathway: A Nonredundant Role in Intestinal Damage in Mice Through a TWEAK/Intestinal Epithelial Cell Axis

TAEKO DOHI,* ANNA BORODOVSKY,‡ PING WU,‡ JEFFREY R. SHEARSTONE,‡ REI KAWASHIMA,* LAURA RUNKEL,‡ LUIS RAJMAN,‡ XINGWEN DONG,‡ MARTIN L. SCOTT,‡ JENNIFER S. MICHAELSON,‡ ANIELA JAKUBOWSKI,‡ and LINDA C. BURKLY‡

*Department of Gastroenterology, Research Institute, International Medical Center of Japan, Tokyo, Japan; ‡Departments of Immunobiology and Drug Discovery, Biogen Idec, Cambridge, Massachusetts

Background and Aims: **Tumor necrosis factor (TNF) superfamily members have attracted attention as new therapeutic targets for treating inflammatory disease. TNF-like weak inducer of apoptosis (TWEAK) is a unique, multifunctional TNF family cytokine that signals through its receptor, fibroblast growth factor–inducible molecule 14 (Fn14). The role of this pathway in the intestine has not been previously reported.** ***Methods:*** **The 2,4,6-trinitrobenzene sulfonic acid (TNBS)-induced colitis model was conducted in TWEAK- or Fn14-deficient mice or in normal mice treated with a TWEAK-blocking monoclonal antibody, and clinical severity, histopathology, immunohistochemistry for cell infiltrates, TWEAK and Fn14, gene expression profiling in the colon, and systemic adaptive immunity were assessed. The effect of TWEAK on colon epithelial cell production of inflammatory mediators was analyzed in vitro. The γ-irradiation injury model was conducted in TWEAK- or Fn14-deficient mice, and crypt epithelial death was assessed.** ***Results:*** **Colitis severity and histologic scores were significantly reduced by TWEAK pathway deficiency or TWEAK-blocking monoclonal antibody. Neutrophil and macrophage infiltrates, chemokines, cytokines, and matrix metalloproteinase expression were reduced in the TWEAK-deficient colon after TNBS administration; however, systemic adaptive immune responses to trinitrophenyl were not altered. Fn14 is expressed on colon epithelial cells in TNBS colitis, and TWEAK induces epithelial production of pathogenic mediators. TWEAK also regulates intestinal epithelial turnover, as evidenced by reduced epithelial cell death after γ-irradiation injury in TWEAK and Fn14 knockout mice.** ***Conclusions:*** **Our studies elucidate a nonredundant TWEAK-intestinal epithelial cell axis and suggest that blocking TWEAK may dampen chronic intestinal inflammation and allow normal epithelial repair.**

BASIC—ALIMENTARY TRACT

The tumor necrosis factor (TNF) superfamily of cytokines includes well-known regulators of immunity and organogenesis.[1] Tumor necrosis factor–like weak inducer of apoptosis (TWEAK) is a member of the TNF family that is highly expressed by inflammatory cells, including activated T cells and innate immune cell types.[2,3] Like TNF, TWEAK is a type II transmembrane homotrimer that can function as a soluble cytokine with diverse biological roles, including proinflammatory activity, angiogenesis, and regulation of cell survival, proliferation, and death.[4] TWEAK mediates these effects through its receptor, fibroblast growth factor–inducible molecule 14 (Fn14),[5] which is expressed by epithelial, mesenchymal, and endothelial cells, as well as by progenitor cells,[4] and signals via the nuclear factor-κB and mitogen-activated protein kinase pathways.[6,7] Interestingly, Fn14 expression is highly up-regulated in contexts of tissue injury and regeneration, and chronic inflammatory disease, supporting a physiologic role for this pathway in coordinating acute inflammation and tissue repair and a pathologic role in chronic disease.[4]

Reports of Fn14 expression in the gastrointestinal tract are limited, with moderate messenger RNA (mRNA) levels observed in normal human tissue mRNA arrays.[8] However, expression of Fn14 is well documented in cells of epithelial origin such as bronchial, mammary, and bile duct epithelium and human keratinocytes.[9-12] Several colon carcinoma cell lines constitutively express Fn14.[13,14] These observations prompted us to investigate Fn14 expression in the gastrointestinal tract and potential involvement of TWEAK/Fn14 in models of intestinal epithelial damage and repair. Several nonmutually exclusive functions of this pathway are possible: TWEAK may regulate proliferation versus death of mature epithelium or crypt progenitors, thereby impacting repair; and TWEAK may be proinflammatory[4] or repress innate im-

Abbreviations used in this paper: Fn14, fibroblast growth factor–inducible molecule 14; Ig, immunoglobulin; IL, interleukin; KC, keratinocyte-derived chemokine; KO, knockout; mAb, monoclonal antibody; MCP, monocyte chemoattractant protein; MMP, matrix metalloproteinase; mRNA, messenger RNA; NK, natural killer; TNBS, 2,4,6-trinitrobenzene sulfonic acid; TNF, tumor necrosis factor; TNFR, TNF receptor; TNP, trinitrophenyl; TWEAK, tumor necrosis factor–like weak inducer of apoptosis; WT, wild-type.

0016-5085/09/$36.00
doi:10.1053/j.gastro.2008.11.017

munity.[3] Thus, blocking the TWEAK pathway might be beneficial, deleterious, or have no effect on the outcome depending on the particular context.

We studied the role of the TWEAK/Fn14 pathway in 2 murine models of intestinal damage. 2,4,6-Trinitrobenzene sulfonic acid (TNBS)-induced colitis is a model of human inflammatory bowel disease in which intrarectal instillation of TNBS with ethanol injures the epithelial barrier, followed by a T cell–mediated immune response against haptenated colonic proteins, leading to mucosal inflammation and epithelial damage involving both innate and adaptive immune components. The γ-irradiation injury model induces much more limited damage directed at the rapidly dividing progenitor cells of the intestinal crypts without a significant inflammatory component.[15,16]

Our studies elucidate the TWEAK/Fn14 pathway as a novel pathogenic mediator in models of intestinal injury, promoting pathology through its effects on epithelial cell inflammatory responses and turnover. TWEAK deficiency limits local intestinal pathology without impairing systemic adaptive immune responses.

Materials and Methods

Mice

TWEAK or Fn14 knockout (KO) mice were backcrossed onto Balb/c or C57BL/6 backgrounds for 5–6 generations under specific pathogen-free conditions at Biogen Idec or the International Medical Center of Japan. All experimental protocols were approved by the institutional animal care and use committees.

Generation of TWEAK- and Fn14-Deficient Mice

TWEAK KO mice were generated as described,[17] and lack of TWEAK mRNA expression was confirmed by reverse transcription–polymerase chain reaction and Northern blot using the full length TWEAK complementary DNA, and glyceraldehyde-3-phosphate dehydrogenase probed as a control. Generation of Fn14 KO mice was described.[9]

Induction and Evaluation of Colitis

TNBS colitis was induced by intrarectal administration of a 2% solution of TNBS in phophate-buffered saline:ethanol (1:1).[18,19] For acute inflammatory responses, 60 μg/g body weight of TNBS was given on day 0, and animals were killed on day 3. For late-phase responses, 36 μg/g body weight of TNBS was administered on days 0 and 7, and animals were killed on day 10. Clinical severity was scored as follows: 0, normal stool; 1, soft stool; 2, diarrhea or proctitis (macroscopically visible perianal erosions and ulcers); 3, anal bleeding; 4, found dead or killed due to moribund condition. In some studies, mice were treated with murine anti-TWEAK monoclonal antibody (mAb) P2D10[17] or isotype-matched control P1.17 (ATCC, Manassas, VA), 300 μg on days 3 and 7, with mice killed on day 10, or as otherwise specified.

Histologic Evaluation

The colons of surviving mice were cut into proximal, middle, and distal segments. Tissue was formalin-fixed and paraffin-embedded, and 4- μm sections were stained with H&E. Each colon segment was scored individually, and these scores were summed to reach a total score for the entire colon. Histologic scores were assigned to each segment as follows: 0, normal; 1, ulcer or cell infiltration limited to the mucosa; 2, ulcer or limited cell infiltration in the submucosa; 3, focal ulcer involving all layers of the colon; 4, multiple lesions involving all layers of the colon, or necrotizing ulcer larger than 3 mm in length. Thus the total possible histologic score is 12.

γ-Irradiation Protocol

Mice received 3 Gy of whole-body irradiation using the γ-irradiation apparatus MBR-1520-R (Hitachi Medical Corp, Tokyo, Japan). Small intestine and colon were collected at 24 hours postirradiation. Paraffin-embedded sections were prepared from a Swiss roll of whole colon or a 7-cm length from the oral end of the small intestine for analysis of jejunum. Numbers of apoptotic cells per crypt, detected in H&E-stained sections by chromatin condensation, were counted in 20 separate crypts in 3 or more fields for each animal.

Immunohistochemistry

Frozen colon sections, 4-μm thick, were cut from a Swiss roll of the whole colon, fixed with cold acetone for 20 minutes, treated with BlockAce (Dainippon Pharmaceutical Co, Ltd, Osaka, Japan) for 20 minutes at room temperature, the Avidin-biotin blocking kit (Vector Labs, Burlingame, CA), and then biotinylated anti-Fn14 mAb (P3D8) (1 μg/mL in 0.2% BlockAce; Invitrogen, San Diego, CA)[20] for 2 hours at room temperature, and detected with Alexa488-labeled streptavidin (1:500 dilution; DS Pharma Biomedical Co, Ltd, Osaka, Japan) for 30 minutes. Images were captured with a fluorescence microscope (BX50/BXFLA; Olympus, Tokyo, Japan) with a CCD camera and merged using Adobe Photoshop CS2 (Adobe Systems, Inc, San Jose, CA). Fixed frozen sections were stained with biotinylated anti–Gr-1 mAb or anti-F4/80 followed by phycoerythrin-streptavidin (BD Biosciences, San Jose, CA), and directly incubated with substrate 3,3′-deaminobenzidine tetrahydrochloride in the presence of hydrogen peroxide to detect myeloperoxidase activity.

Sacral Lymph Node T-Cell Responses

Cells isolated from sacral lymph nodes were treated with 0.3 mg/mL TNBS in RPMI 1640 for 15 minutes at room temperature, extensively washed, and cultured in complete medium for 3 days at a density of

2×10^5 cells/well. [^{3}H] Thymidine, 0.5 μCi, was added to each well 18 hours before harvesting and scintillation counting.

Serum Anti-trinitrophenyl Titer

Sera were collected on day 10, assayed on microtiter plates coated with trinitrophenyl (TNP)-coupled ovalbumin, with detection by peroxidase-labeled secondary antibodies against mouse immunoglobulin (Ig) isotypes (Southern Biotechnology Associates Inc, Birmingham, AL). Endpoint titers were expressed as the reciprocal log2 of the last dilution, which gave an optical density of 0.1 greater than the pooled serum obtained from naïve mice of the same strain.

Total RNA Isolation for Gene Profiling

Colon middle and distal segments were resuspended in TRIzol (Invitrogen Life Technologies, Carlsbad, CA), and homogenized and further purified using an RNeasy Mini column (QIAGEN, Valencia, CA).

Gene Expression Profiling and Analysis

Samples were profiled using the Mouse Genome Mouse 430 2.0 GeneChip probe array according to the manufacturer's protocol (Affymetrix, Santa Clara, CA) and supplemental information.

Colon Epithelial In Vitro Cultures

The SV40 immortalized, nontransformed cell lines MODE-K[21] and MCE301[22] were cultured with media alone, or with specified concentrations of murine soluble TWEAK, soluble Fn14 plus soluble TWEAK, an agonistic anti-Fn14 mAb P2.D3, or isotype-matched control Ig, MOPC-21, for 24 hours. Culture supernatants were analyzed by SearchLight multiplex enzyme-linked immunosorbent assay (Pierce Boston Technology Center, Woburn, MA) for chemokines, cytokines, and matrix metalloproteinases (MMPs).

Methods for supplementary figures are provided in the Supplementary Methods section; see supplementary material online at www.gastrojournal.org.

Results

Fn14 mRNA Is Increased in TNBS-Treated Colons of Balb/c Mice

To explore the role of the TNF superfamily in murine TNBS colitis, a gene profiling study was conducted with Balb/c colons collected 3 days after intrarectal TNBS/ethyl alcohol to determine acute changes in gene expression. Alternatively, animals were given a second dose of TNBS on day 7, and colons were collected 3 days later (day 10) to examine the later phase of the pathology. Three members of the TNF receptor (TNFR) superfamily showed significant up-regulation in colons of TNBS-treated mice in comparison with untreated controls in both the acute and late stages of colitis (Supplementary Figure 1; see supplementary material online at www.gastrojournal.org). Expression of TNFR1 and 2 was increased; however expression of their ligand TNFα was not detected, consistent with the prior report of no effect of TNF blockade in TNBS-induced colitis in the Balb/c strain.[23] Interestingly, a similar up-regulation of Fn14, the TWEAK receptor, was also observed, and mRNA of TWEAK was expressed in both the normal and inflamed colon, suggesting a role for the TWEAK/Fn14 pathway in TNBS-induced colitis.

TWEAK KO Animals Have a Normal Immune System and Intestinal Architecture

To study the role of the TWEAK/Fn14 pathway in TNBS colitis, we used TWEAK KO mice (Supplementary Figure 2*A*; see supplementary material online at www.gastrojournal.org).[17] Lack of TWEAK expression was confirmed by Northern blot (Supplementary Figure 2*B*; see supplementary material online at www.gastrojournal.org). Expression of genes neighboring the TWEAK locus was unaltered (Supplementary Figure 3; see supplementary material online at www.gastrojournal.org).

TWEAK-deficient animals were healthy and normal. Comprehensive necropsy revealed no abnormalities, and extensive immune compartment analysis showed normal spleen weights in both young and aged mice, and normal percentages and absolute numbers of splenic B, T, natural killer (NK), and NK T-cell subsets and activated/memory cells within the CD4 and CD8 T-cell populations (Supplementary Figure 2*C–E*; see supplementary material online at www.gastrojournal.org). Baseline levels of Ig subclasses were also comparable to those of wild-type (WT) mice (data not shown). Intestines of TWEAK KO and previously described Fn14 KO mice[9,24] were normal in gross morphology and histology (see below). WT and TWEAK KO colons also showed comparable gene expression profiles with no statistically significant differences, suggesting that this pathway does not play a major role in the normal homeostasis of the gastrointestinal tract.

TWEAK KO Mice Are Protected From TNBS-Induced Colitis and Display Reduced Mucosal Ulceration

After colonic TNBS administration, WT animals displayed wasting disease accompanied by bloody diarrhea and, in some animals, rectal obstruction. Substantial mortality was observed; however, TWEAK KO animals tended to survive in greater numbers (12 of 15) than WT controls (8 of 16) (Figure 1*A*). TWEAK KO animals exhibited a significant reduction in weight loss (Figure 1*B*) along with a significantly reduced clinical score (Figure 1*C*). These results indicate a significant protective effect of TWEAK deficiency in the TNBS-induced colitis model.

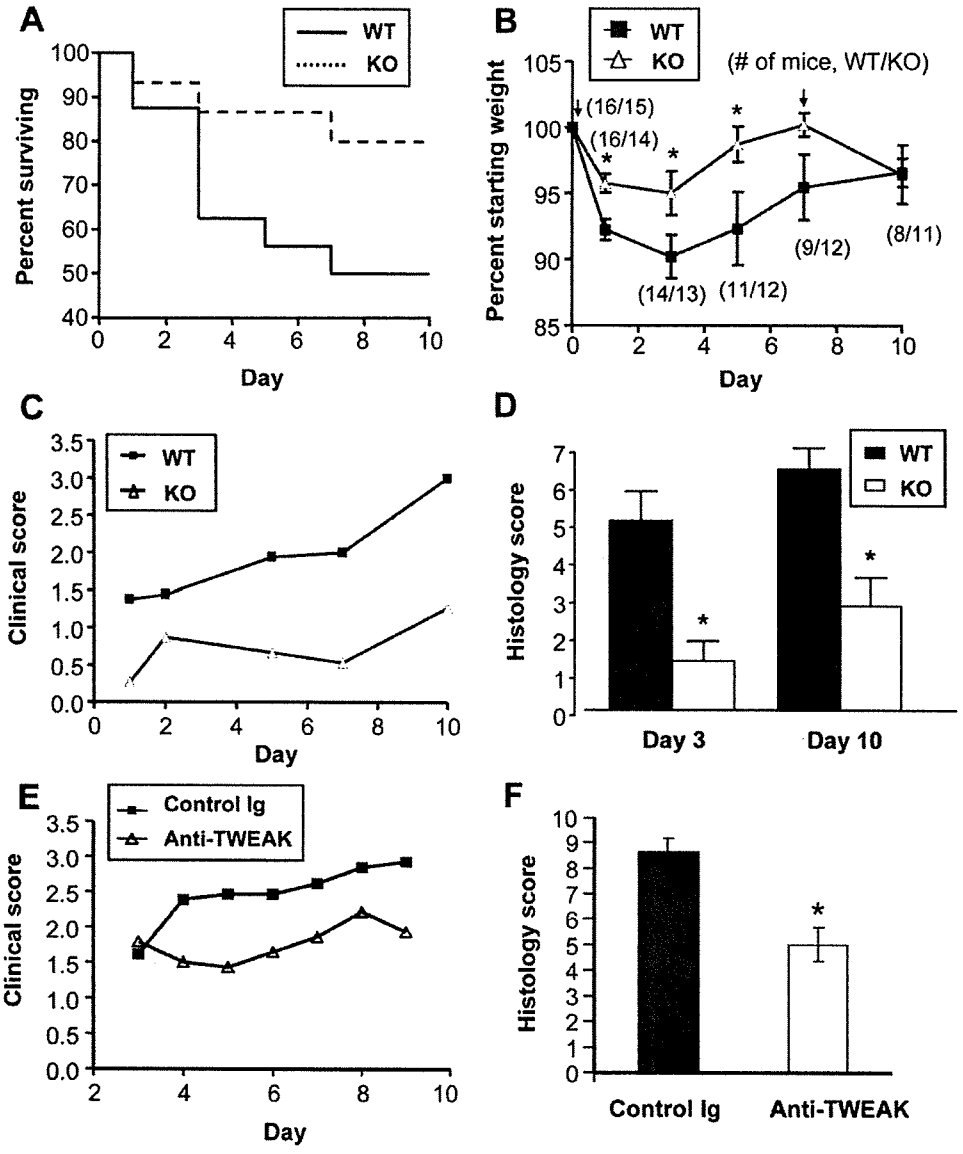

Figure 1. TNBS-induced colitis in Balb/c TWEAK KO and anti-TWEAK mAb–treated mice. (*A*) Survival curves for TWEAK KO (*dotted line*, n = 15) and WT mice (*solid line*, n = 16) after TNBS treatment on days 0 and 7. Kaplan-Meier analysis, P = .086. (*B*) Mean weight loss (±SEM) in TWEAK KO and WT mice after TNBS treatment on days 0 and 7 (indicated by *arrows*). The number of WT and KO mice for each time point are in parentheses. *Asterisks* indicate significant differences (P < .05, Student's two-tailed t test) on days 1, 3, and 5. (*C*) Mean clinical score in TWEAK KO (n = 16) and WT (n = 15) mice. Difference between the groups was significant; 2-way analysis of variance (ANOVA) P < .0001. (*D*) Mean histology scores (±SEM) for surviving mice on day 3 (n = 7 per group) or day 10 for WT (n = 8) and TWEAK KO (n = 12). *Asterisks* indicate P < .01 by Mann-Whitney test. (*E*) Mean clinical scores in Balb/c mice treated with anti-TWEAK mAb (n = 14) or control Ig (n = 13) starting on day 3 after TNBS administration. Difference between the groups was significant; 2-way ANOVA P = .0014. (*F*) Mean histology scores (±SEM) for colons of surviving mice treated with anti-TWEAK antibody or control Ig starting on day 3 after TNBS administration and killed on day 10 (anti-TWEAK, n = 8; control Ig treated, n = 5). *Asterisks* indicate significant P values by Mann-Whitney test, P = .0062.

WT Balb/c animals displayed typical colonic macroscopic and histologic features associated with TNBS colitis, including colon wall thickening and focal ulcers in the mucosa of the distal half of the colon (Figure 2).[19] Loss of goblet cells, mononuclear cell infiltration, and crypt distortion were also observed. TWEAK KO mice displayed reduced epithelial ulceration and infiltrate levels and corresponding reductions in crypt deformity as compared with WT on day 10 (Figure 2). TWEAK KO mice exhibited a significantly lower histologic score than WT controls (Figure 1*D*), reflecting 2 prominent differences on both days 3 and 10: a reduction in frequency and extent of epithelial ulcers, and a reduction in leukocyte infiltration into the submucosa. The overall magnitude of inflammatory cell infiltration was also reduced in TWEAK KO as compared with WT colons at both the early and late disease stages (Supplementary Figure 4; see supplementary material online at www.gastrojournal.org).

TNBS colitis was also induced in TWEAK- or Fn14-deficient mice on the C57BL/6 background. A similar protective effect was seen in this strain in the absence of either TWEAK or Fn14 (Supplementary Figure 5; see supplementary material online at www.gastrojournal.org). In addition, WT Balb/c mice were treated with an anti-TWEAK blocking antibody starting either on day 0 (Supplementary Figure 6; see supplementary material online at www.gastrojournal.org) or starting 3 days after TNBS administration, and diminished clinical score and histologic damage to the colon likewise were observed (Figure 1*E* and *F*). Taken together, our studies indicate that the TWEAK/Fn14 pathway contributes to both the onset and progression of TNBS-induced colitis.

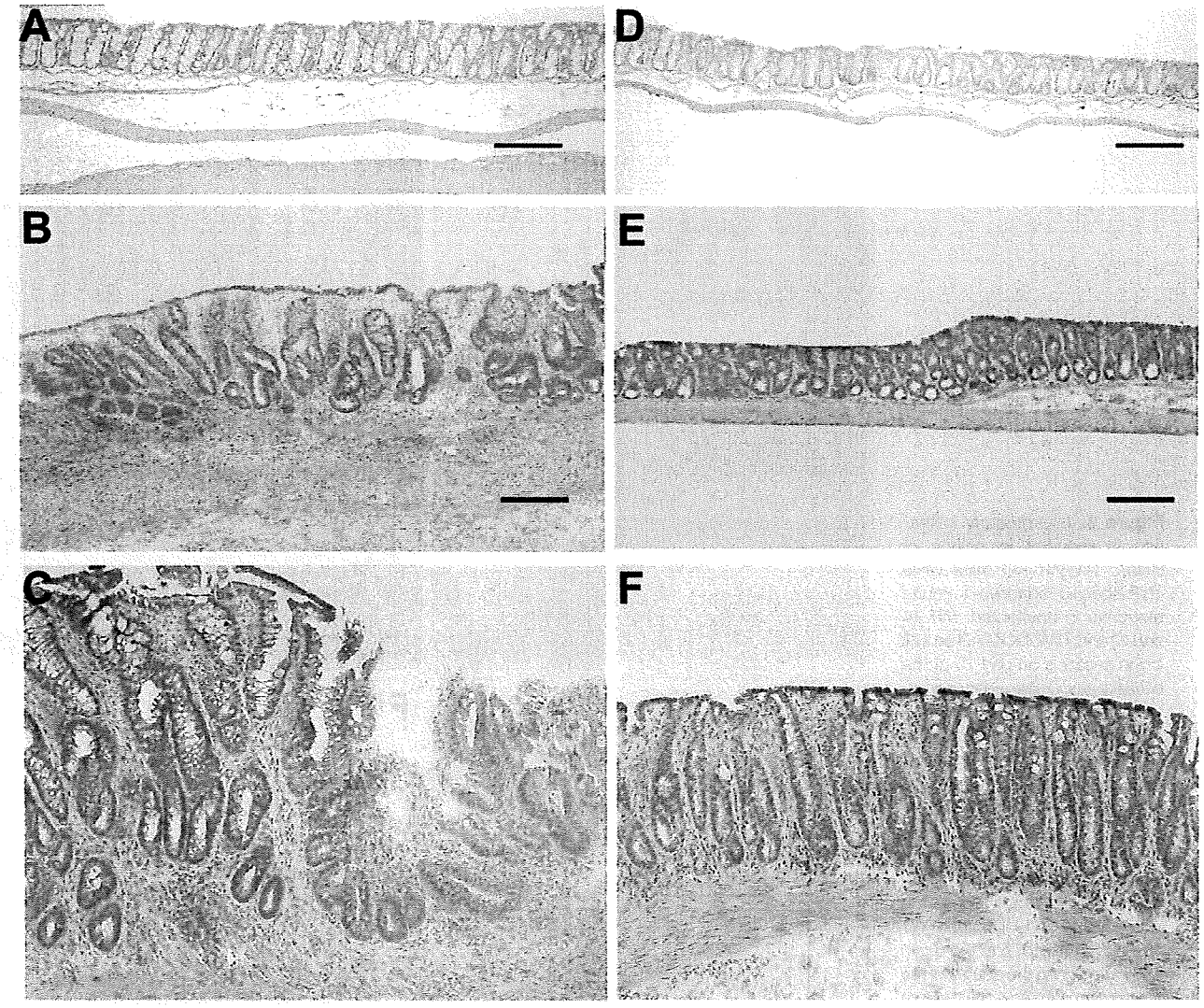

Figure 2. Histologic damage is reduced in Tweak KO. Histologic features of Balb/c WT and TWEAK KO colons: untreated WT (*A*) and KO (*D*), and from day 10 of the TNBS-colitis protocol, TWEAK WT (*B* and *C*) and KO (*E* and *F*). *Scale bars* in *A*, *B*, *D*, and *E* correspond to 0.1 mm. *C* and *F* images are 2-fold higher magnification than *B* and *E*.

Infiltration Is Reduced but the Adaptive Immune Response Is Not Altered in TWEAK KO Mice

The mucosal damage induced by a TNBS/ethyl alcohol enema leads to extensive neutrophil and macrophage infiltrates that persist and secrete proinflammatory mediators and reactive oxygen species that contribute to tissue damage. TWEAK KO mice exhibited a significantly reduced level of peroxidase activity (Figure 3*A* and *B*), and staining for neutrophil marker Gr-1 (data not shown) was likewise diminished. Monocyte infiltration was also reduced in TWEAK KO colons (Figure 3*C* and *D*).

TNBS colitis is also associated with a robust adaptive immune response to TNP-modified proteins. TWEAK deficiency did not alter generation of the TNP-specific T-cell response in draining sacral lymph nodes (Figure 3*E*), or serum levels of anti-TNP antibodies (Figure 3*F*). These findings suggest that TWEAK deficiency ameliorates local pathogenic events rather than the systemic adaptive immune component.

Expression of Inflammation and Neutrophil/Monocyte-Related Genes Is Reduced in the Colons of TNBS-Treated TWEAK KO Mice

To investigate the basis for protection from colitis in TWEAK KO mice at a molecular level, gene profiling was conducted with colons from acute (day 3) or late-stage (day 10) colitis or untreated control animals. No significant differences in gene expression were observed between untreated KO and WT colons. Overall, 638 genes exhibited a statistically significant change in expression

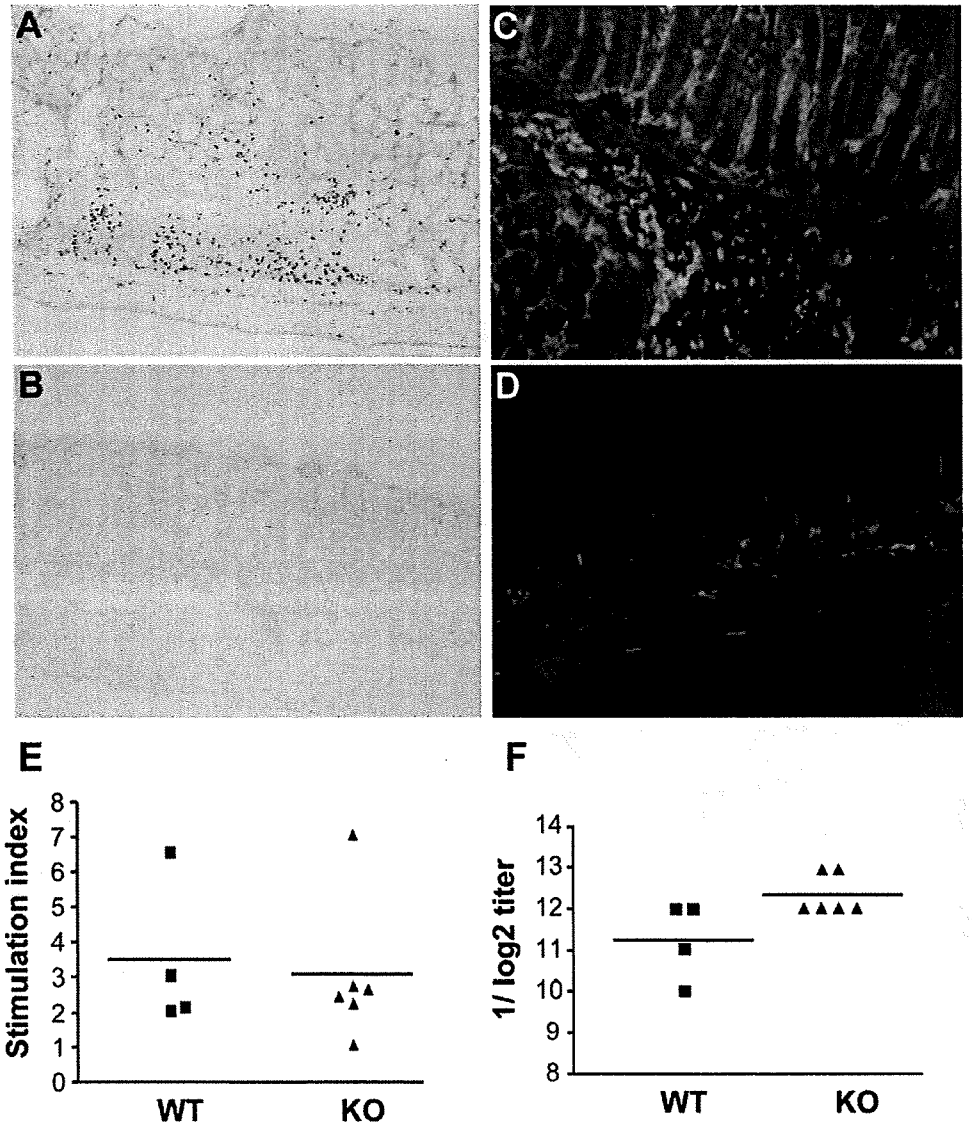

Figure 3. Inflammatory infiltration is reduced in colons of Balb/c TWEAK KO mice while TNP-specific adaptive immune response is unaffected. WT (*A* and *C*) and TWEAK KO (*B* and *D*) colon sections on day 10 of the colitis protocol stained for peroxidase activity (*A* and *B*) or macrophage marker F4/80 (*C* and *D*). Images are representative of results obtained in n = 8 mice per group. (*E*) Anti-TNP response of sacral lymph node T cells on day 10; stimulation index calculated as the level of in vitro ^{3}H-thymidine incorporation compared with cultures without antigen. WT group is smaller due to the death of 3 mice during the course of the experiment. (*F*) Anti-TNP serum IgG titer on day 10 of TNBS colitis. No significant differences.

of greater than 2-fold in WT colons on day 3 as compared with only 239 gene changes in TWEAK KO. A similar trend was observed at day 10. A group of genes expressed by neutrophils and macrophages was present at a greatly reduced level in TWEAK-deficient colons on both days 3 and 10 (Table 1), consistent with the reduced number of infiltrating cells (Figure 3).

Interestingly, profiling revealed differences in the molecular signatures of WT and KO colons that were not shown by histology (Table 1). Expression of 12 genes encoding chemokines/chemokine receptors was markedly reduced in TWEAK KO colons. Most of the chemokines affected were those involved in neutrophil and monocyte chemotaxis. Some of these chemokines are known to be secreted by colon epithelial cells (CXCL1, CXCL5, CCL2), while others are produced by activated macrophages (CXCL2, CCL3) and serve to recruit additional cells into the tissue.[25] In addition, 2 acute-phase cytokines, interleukin (IL)-6 and IL-1β, previously associated with colonic inflammation,[26] were greatly decreased in TWEAK KO mice. Also reduced were MMPs and their inhibitors, enzymes important for turnover of extracellular matrix proteins and cell migration, whose expression is associated with inflammation and subsequent tissue repair.[27]

Fn14 Is Expressed by Colon Epithelial Cells in TNBS Colitis, and TWEAK Induces Colon Epithelial Cell Production of Inflammatory Mediators

To further define the pathogenic mechanism of TWEAK in TNBS colitis, we identified cells expressing TWEAK and its receptor, Fn14. TWEAK was expressed by intestinal epithelial cells in WT tissue (Supplementary

Table 1. Fold Change in Gene Expression in WT and TWEAK KO Colons Treated With TNBS Relative to Untreated Animals

	Gene name (s)[a]	Function/description	Day 3[b]		Day 10[c]	
			WT	KO	WT	KO
Chemokines	CXCL2 (MIP-2)	Neutrophil recruitment	113.2	3.0	24.2	6.7
	CXCL1 (KC)	Neutrophil recruitment	50.6	2.4	19.3	4.1
	CXCL5 (LIX)	Neutrophil recruitment	36.1	1.9	13.6	4.5
	CCL3 (MIP-1α)	Monocyte/Th1 chemotaxis	19.2	ns	6.8	3.0
	CCL2 (MCP-1)	Monocyte recruitment	7.3	ns	3.2	1.7
	CCL7 (MCP-3)	Pluripotent/leukocyte activation	6.1	ns	3.2	1.9
	CXCL4 (PF4)	Inhibitor of angiogenesis	5.3	1.4	2.4	1.7
	CCL11 (Eotaxin)	Eosinophil recruitment	4.8	ns	3.5	1.6
	CCL9	Neutrophil, monocyte, CD4 chemotaxis	4.3	ns	2.5	1.7
	CCL24	Eosinophil recruitment	2.8	ns	2	ns
Chemokine receptors	CCR1	Monocyte/lymphocyte chemotaxis	5.0	3.9	1.4	2.3
	CCR5	Monocyte/Th1 T-cell chemotaxis	3.5	2.9	1.5	2.1
Cytokines/receptors	IL-6	Acute-phase response	23.6	ns	8.4	2.2
	IL-1β	Leukocyte activation	16.7	1.3	10.2	3.3
	IL-15	Monocyte/neutrophil activation, CD8 NK survival	−2.7	−1.3	−1.3	−1.3
	IL-1Rβ	IL-1 decoy receptor	9.8	1.4	4.0	2.6
Neutrophil/macrophage genes	S100A8	Major neutrophil cytosolic protein	123.0	5.3	39.8	14.4
	S100A9	Major neutrophil cytosolic protein	105.3	4.9	35.7	12.9
	PTX3	Acute phase, secreted by macrophages	23.1	1.4	5.8	1.9
	Mcl	Macrophage lectin	18.0	1.4	7.2	3.3
	Mincle	Macrophage lectin induced by inflammation	17.6	1.8	5.6	2.4
	CD11b	Macrophage integrin αM	9.8	ns	3.9	2.0
	CD157	Neutrophil adhesion/chemotaxis	6.6	ns	3.7	1.5
	CD68	Macrophage marker	5.6	1.7	3.1	2.0
	NCF4	Neutrophil cytosolic factor 4	4.5	1.5	3.2	2.1
	GM-CSFR	Macrophage activation/maturation	4.4	1.5	2.8	1.5
MMP	TIMP-1	Tissue inhibitor of metalloproteinases	30.1	1.8	9.6	4.2
	MMP-13	Collagenase, ECM remodeling	16.9	ns	10.1	2.4
	MMP-9	Gelatinase, ECM remodeling	11.8	1.6	7.2	3.0
	MMP-3	Stromelysin, ECM remodeling	8.9	ns	4.6	2.2
	MMP-10	Stromelysin, ECM remodeling	6.5	1.4	4.0	1.6
	ADAM-8	CD156, monocytic lineage cells	6.4	ns	3.4	1.7
	MMP-12	Metalloelastase, ECM remodeling	6.1	ns	4.9	2.0
	ADAM-12	Meltrin-α, ECM remodeling	3.3	ns	2.9	1.4

ADAM, a disintegrase and metalloproteinase; CCL, CC chemokine ligand; CXCL, chemokine ligand; CCR, CC chemokine receptor; ECM, extracellular matrix; GM-CSFR, granulocyte-macrophage colony-stimulating factor receptor; LIX, lipopolysaccharide-induced CXC chemokine; Mcl, macrophage C-type lectin; Mincle, macrophage-inducible C-type lectin; MIP, macrophage inflammatory protein; PF, platelet factor; PTX-3, pentraxin-related gene; ns, no significant difference with untreated; Th1, T helper 1.

[a]Genes listed are those for which a significant difference is observed between TNBS-treated KO and WT in acute colitis samples (day 3).

[b]Colons from animals euthanized 3 days after TNBS treatment versus untreated.

[c]Colons from animals treated with TNBS on days 0 and 7 and euthanized on day 10 versus untreated. Italicized fold-changes have a random variance *t* test *P* value between .01 and .05, *P* values are less then .01 for all others, for treated animals compared with untreated controls.

Figure 7; see supplementary material online at www.gastrojournal.org), whereas expression by other cell types was equivocal, warranting further investigation. TWEAK expression was similar before and 3 days after disease induction. In contrast, there was little if any Fn14 in normal WT colon (Figure 4*A*), whereas Fn14 expression by colon epithelial cells was markedly increased in WT mice 3 days after TNBS administration (Figure 4*B*). Double staining for Fn14 and epithelial cell adhesion molecule (EpCAM) confirmed the epithelial localization, and for Fn14 and F4/80 indicated that Fn14 was not expressed by the colon-infiltrating macrophages (Supplementary Figure 8; see supplementary material online at www.gastrojournal.org). The potential mechanism for up-regulation of Fn14 was explored using colon tissue cultures stimulated with inflammatory cytokines or bacterial products. Our results suggest that Fn14 expression can be induced by exposure to a cytosine guanine dinucleotide (CpG) containing oligodeoxynucleotide (CpG ODN) (Supplementary Figure 9; see supplementary material online at www.gastrojournal.org).

To directly demonstrate whether TWEAK can stimulate intestinal epithelial cells to produce proinflammatory mediators, we used cell lines that express Fn14 (Figure 5*A*). Culture of MODE-K cells with TWEAK significantly increased MMP-9 production. This stimulatory effect of TWEAK is mediated by Fn14, as supported by the ability of soluble Fn14 to block it, as well as by the

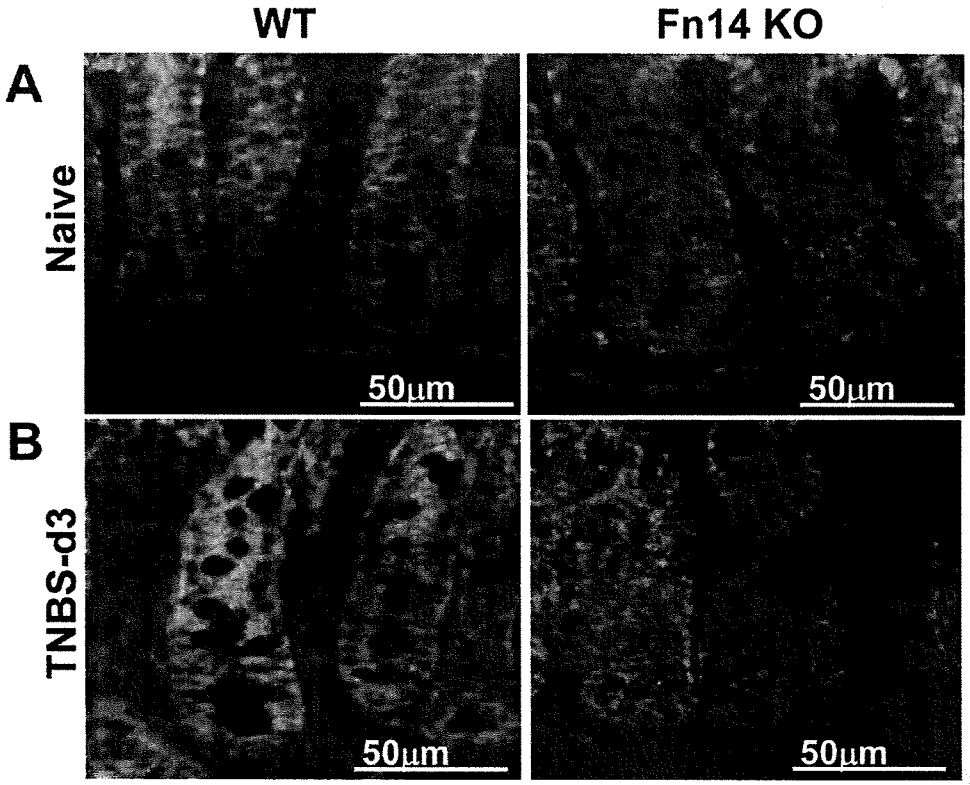

Figure 4. TWEAK receptor, Fn14, is expressed by colon epithelial cells. Anti-Fn14 immunofluorescent staining (*green*) of colon sections from Balb/c WT and Fn14 KO mice untreated (*A*) and 3 days after TNBS colitis (*B*). Luminal edge tissue showed nonspecific staining in both WT and KO as shown in *A*.

direct stimulatory effect of ligating the cell surface Fn14 receptor with an Fn14-specific agonist mAb (Figure 5*B*). This direct approach was further used to demonstrate Fn14-mediated induction of CXCL1 (also known as keratinocyte-derived chemokine [KC]) and CCL2 (also known as monocyte chemoattractant protein-1 [MCP-1]) (Figure 5*C*). There was a tendency to induce IL-6; an array of other mediators, including IL-1β and TNFα, were unchanged (not shown). TWEAK stimulation of proinflammatory mediator production was also observed with the MCE301 cell line (Supplementary Figure 10; see supplementary material online at www.gastrojournal.org). These results suggest that TWEAK acts locally through Fn14-expressing epithelial cells to promote pathogenic tissue inflammation and matrix remodeling in TNBS colitis.

TWEAK/Fn14 Pathway Deficiency Is Protective in a γ-Irradiation–Induced Model of Intestinal Epithelial Damage

To determine whether TWEAK and Fn14 also regulate intestinal epithelial turnover, we used a γ-irradiation model of epithelial damage, which has a less prominent inflammatory component and allows one to visualize apoptosis in the rapidly dividing epithelial progenitor cells of the intestinal crypts, followed by renewed proliferation of surviving crypt progenitors.[16]

Balb/c TWEAK KO mice showed a significantly lower number of apoptotic cells than WT in both jejunum and colon after whole-body irradiation (Figure 6*A–E*). In WT mice, a relatively high frequency of apoptotic cells was found in the lower crypt positions on the longitudinal crypt axis (Figure 6*F*) where small intestine crypt progenitor cells are localized,[16] although increased apoptosis was also observed at higher crypt positions. TWEAK KO mice display a marked reduction in the percentage of apoptotic cells at both lower and higher crypt positions (Figure 6*F*). The reduction in apoptosis after γ-irradiation injury was also observed in Fn14 KO mice, and enhanced survival of intestinal epithelial cells in both TWEAK KO and Fn14 KO mice was reflected by a greater number of proliferating crypt cells (Supplementary Figure 11; see supplementary material online at www.gastrojournal.org). Thus, in the γ-irradiation injury model, TWEAK and Fn14 deficiency result in greater survival of intestinal epithelial cells.

Discussion

Our study identifies the TWEAK/Fn14 pathway as a nonredundant pathogenic mediator in contexts of intestinal injury and inflammatory disease. Significant amelioration of TNBS-induced colitis is observed in TWEAK- or Fn14-deficient mice, and in WT mice treated with TWEAK-blocking mAbs prophylactically or therapeutically. TWEAK-deficient animals show an improved clinical course, reduced colon epithelial ulcers, and less infiltration by granulocytes and macrophages. TWEAK

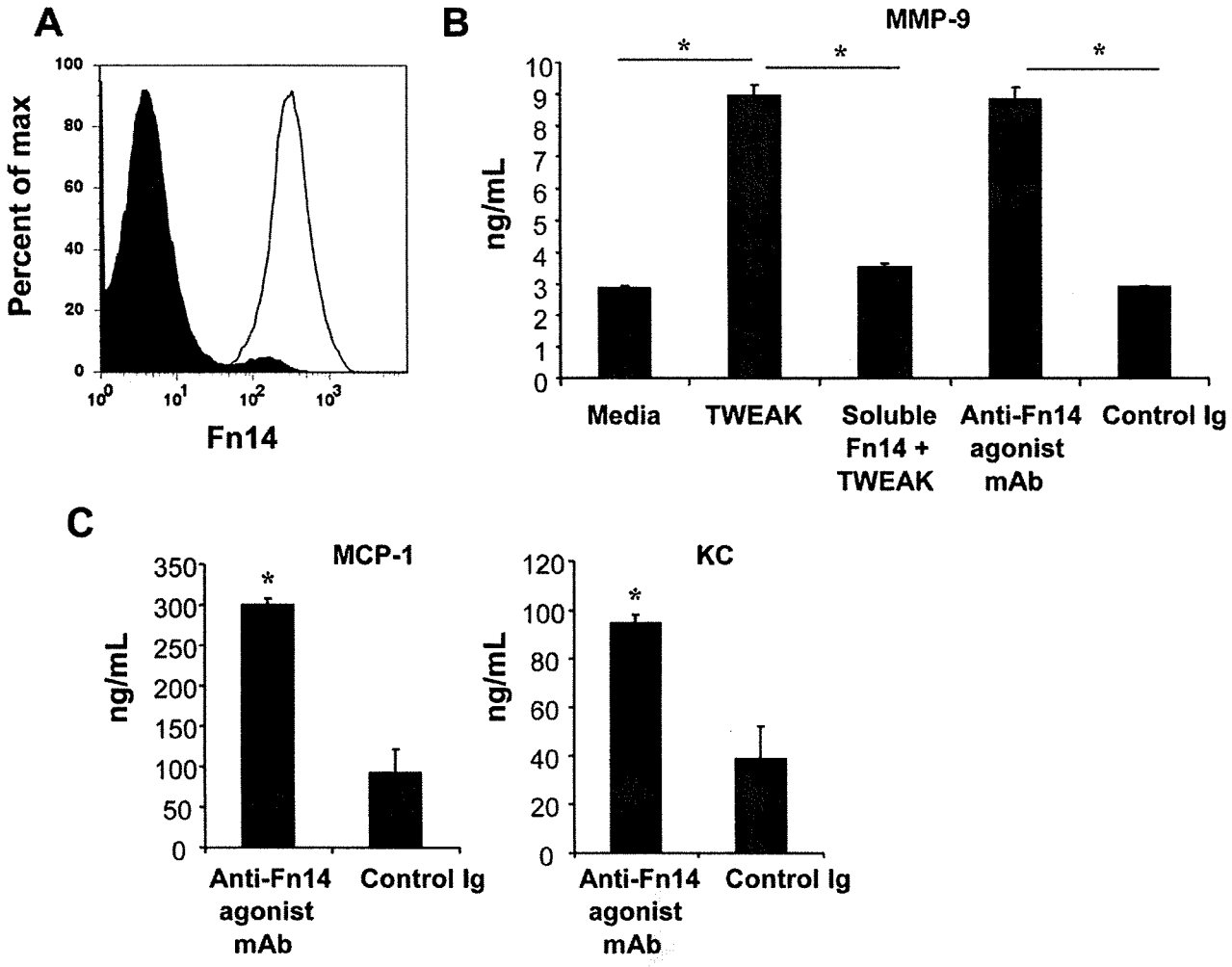

Figure 5. TWEAK/Fn14 induce intestinal epithelial cell production of inflammatory mediators. (*A*) Flow cytometry overlay of anti-Fn14 (*open profile*) versus control Ig staining (*filled profile*) of epithelial cell line MODE-K. (*B*) MMP-9 production by MODE-K cultured in media alone or in the presence of soluble TWEAK (1.0 ng/mL), soluble TWEAK plus soluble Fn14 decoy protein (10 μg/mL), agonistic anti-Fn14 mAb (10 μg/mL), or control Ig (10 μg/mL). (*C*) MCP-1 and KC production stimulated by agonistic anti-Fn14 mAb versus control Ig. Mean values (±SD) are shown for triplicate cultures. *Asterisks* indicate significant differences; all *P* values <.005 by Student two-tailed *t* test.

appears to act locally on intestinal epithelial cells that up-regulate Fn14 after TNBS induction, stimulating production of inflammatory and tissue remodeling enzymes, thereby contributing both acutely and during disease progression to intestinal tissue damage and abnormal tissue repair. TWEAK also regulates epithelial turnover as revealed in the γ-irradiation injury model. In contrast to its contribution to end-organ pathology, TWEAK does not regulate the systemic adaptive response to TNP. Our data suggest that blocking TWEAK may be an intervention point for inhibiting local immune effector mechanisms, as well as controlling epithelial injury, in contexts of intestinal injury and inflammatory disease. Blocking TWEAK may be a favorable intervention point, since it orchestrates events specific to the disease target tissue without systemically impairing host immunity.

Our TWEAK KO mice were extensively characterized, with no differences observed between KO and WT. Since we use full-length TWEAK complementary DNA as a probe in the Northern blot analysis, we are confident that TWEAK expression is completely absent in our animals. However, prior studies in another TWEAK KO strain showed augmented innate immunity and increased numbers of immune cell subsets, including NK and T cells.[3] The differences between the 2 TWEAK-deficient strains are intriguing and might be explained by different housing conditions or distinct targeting strategies for the TWEAK locus, or both. Importantly, the results in our TWEAK KO mice are independently validated in Fn14 KO mice and in WT mice treated with TWEAK-blocking mAb.

Intestinal epithelial cells markedly up-regulate Fn14 after TNBS administration. Although we cannot com-

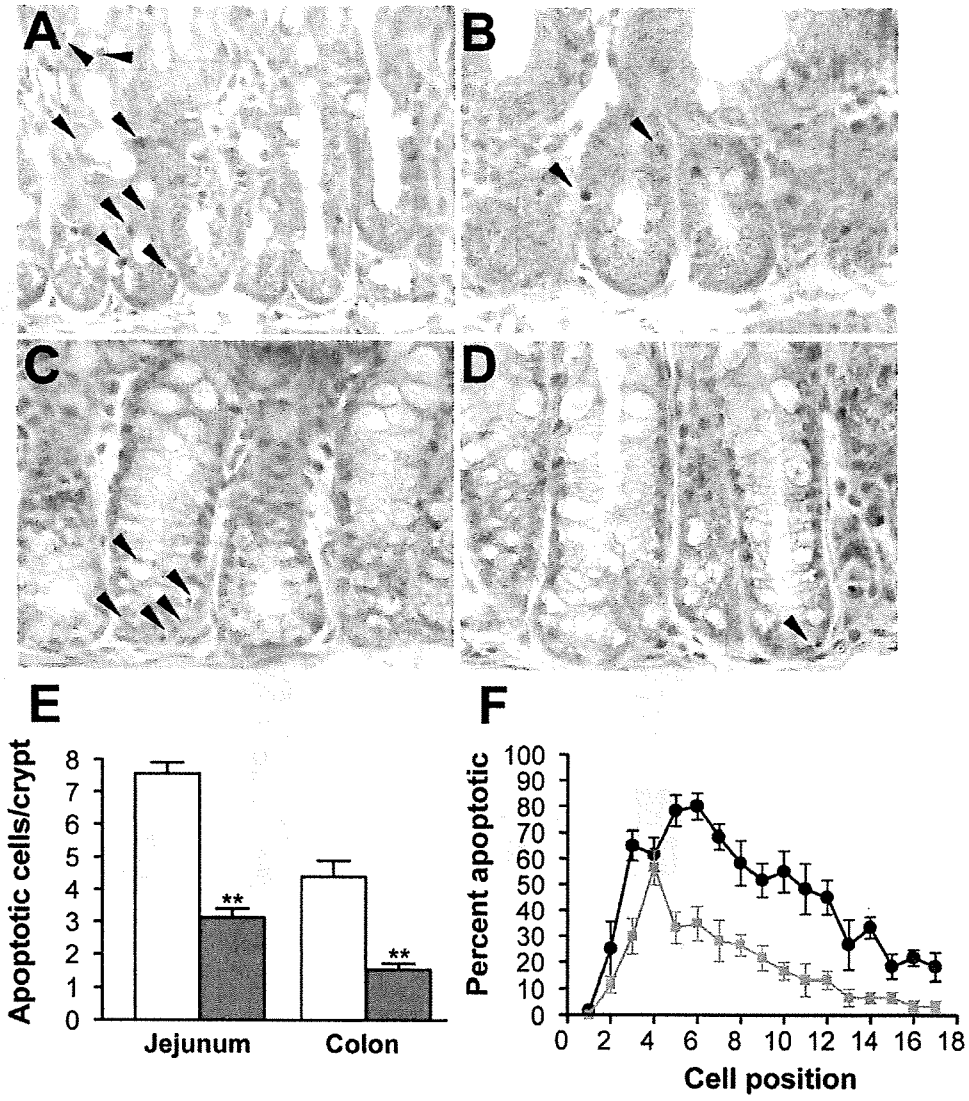

Figure 6. TWEAK deficiency protects small and large intestine crypt epithelium from γ-irradiation-induced apoptosis. Representative H&E-stained images of crypts from BALB/c WT (*A* and *C*) and TWEAK KO (*B* and *D*) jejunum (*A* and *B*) and colon (*C* and *D*) 24 hours after irradiation. Apoptotic cells in a single representative crypt are indicated by *arrowheads*. (*E*) Number of apoptotic cells in the jejunum or colon crypts from Balb/c WT (*white bars*) or TWEAK KO (*gray bars*). *Asterisks* indicate $P < .01$. (*F*) Percentage of apoptotic cells at various crypt positions for Balb/c WT (*black*) versus TWEAK KO (*red*) jejunum. Values shown are mean ± SEM based on analysis of 10–20 crypts for each of the 5 animals per group. All positions (except 1, 2, 4, and 13) showed significant difference between WT and KO; $P < .05$ by Student two-tailed *t* test.

pletely rule out other local Fn14-expressing cells, colon-infiltrating macrophages do not appear to express this receptor. Intestinal epithelium is a well-established player in the innate defense of the intestine.[28] Our in vitro studies suggest that Fn14 may be induced by exposure to bacterial DNA after injury to the epithelial barrier. Although TNFα is not expressed in the Balb/c strain after TNBS administration, it might also induce Fn14 in contexts of intestinal injury on other genetic backgrounds. Intestinal epithelial cells also respond to TWEAK, with increased production of chemokines involved in monocyte and neutrophil recruitment and MMP-9. Conversely, expression of these gene signatures was significantly reduced locally in TWEAK KO as compared with WT colons. While the pathogenic role of inflammatory cytokines, chemokines, and MMPs in models of colitis is well established,[25,27] our studies identify TWEAK as an important instigator of their production in TNBS-induced colitis apparently through stimulation of intestinal epithelial cells. Likewise, TWEAK was previously shown to significantly contribute to joint inflammation and damage in mouse collagen-induced arthritis, likely through its effect on mesenchymal joint cell types, without affecting systemic collagen-specific T-cell antibody responses.[29,30] These studies underscore the important disease-promoting contribution of TWEAK-epithelial and TWEAK-stromal cell interactions locally in the disease target tissue.

MMPs, enzymes important for degradation of extracellular matrix proteins and cell migration, are significantly increased after TNBS administration in WT mice and may contribute to disease pathogenesis in multiple ways. Previously, MMP-9 was shown to be abundantly associated with inflamed areas in ulcer bases in human inflammatory bowel disease tissue,[31] and MMP-3 was shown to produce severe tissue injury in gut explant cultures.[32] Thus, proteolysis by MMPs may contribute to ulcer for-

mation and severity, and reduced MMPs including MMP-3 and MMP-9 in TWEAK KO animals may contribute to reduced ulceration. MMPs are also involved in accumulation of inflammatory cells into the intestine in TNBS colitis as evidenced by reduced neutrophil accumulation in MMP inhibitor-treated animals.[33,34] Thus, reduced MMP expression in TWEAK KO mice may contribute to decreased inflammation. Interestingly, we previously reported that TWEAK induces MMP-9–dependent proliferation and branching of mammary gland epithelial cells in vitro.[11] Decreased anchorage of epithelial cells as a consequence of matrix degradation may trigger cell proliferation and branching. Likewise, in the case of intestinal epithelium, it is tempting to speculate that TWEAK-induced MMP activity reduces epithelial anchoring and thereby promotes cell proliferation, and crypt deformity and branching, features of abnormal repair observed 10 days after TNBS insult. These features are reduced in TWEAK KO mice.

Studies in the model of γ-irradiation injury, which does not have a prominent inflammatory component, allowed us to dissect the effect of TWEAK on epithelial cell turnover after injury. We found greater survival of epithelial cells in TWEAK and Fn14 KO as compared with WT mice in the lower crypts where progenitors are located, as well as at higher crypt positions. There are several possibilities that we currently cannot distinguish: TWEAK mediates epithelial cell apoptosis, or TWEAK promotes epithelial proliferation, thereby making these cells more susceptible to irradiation-induced death. Thus, further studies are warranted to resolve our novel finding that TWEAK regulates epithelial turnover. In either case, the implication for the colitis context is that blocking TWEAK may also be beneficial in limiting damage or limiting abnormal repair (ie, proliferation resulting in crypt deformity/branching).

In summary, our studies demonstrate that TWEAK produced by adaptive and innate cell types acts on epithelial cells to enhance the local production of well-known inflammatory mediators and tissue remodeling enzymes and to regulate epithelial turnover. Anti-TNFα antibody treatment was a milestone in the therapy of Crohn's disease[35] and now in ulcerative colitis.[36] However, 30%–40% of patients are refractory to this treatment. Thus, new therapeutics are sought to address this unmet need. Future studies are warranted to investigate the potential for blocking TWEAK as a possible candidate target for new biologic therapy for intestinal injury and inflammatory bowel diseases.

Supplementary Data

Note: To access the supplementary material accompanying this article, visit the online version of *Gastroenterology* at www.gastrojournal.org, and at doi: 10.1053/j.gastro.2008.11.017.

BASIC—ALIMENTARY TRACT

References

1. Ware CF. The TNF superfamily. Cytokine Growth Factor Rev 2003; 14:181-184.
2. Kaplan MJ, Lewis EE, Shelden EA, et al. The apoptotic ligands TRAIL, TWEAK, and Fas ligand mediate monocyte death induced by autologous lupus T cells. J Immunol 2002;169:6020–6029.
3. Maecker H, Varfolomeev E, Kischkel F, et al. TWEAK attenuates the transition from innate to adaptive immunity. Cell 2005;123: 931–944.
4. Burkly LC, Michaelson JS, Hahm K, et al. TWEAKing tissue remodeling by a multifunctional cytokine: role of TWEAK/Fn14 pathway in health and disease. Cytokine 2007;40:1–16.
5. Wiley SR, Cassiano L, Lofton T, et al. A novel TNF receptor family member binds TWEAK and is implicated in angiogenesis. Immunity 2001;15:837–846.
6. Brown SA, Richards CM, Hanscom HN, et al. The Fn14 cytoplasmic tail binds tumour-necrosis-factor-receptor-associated factors 1, 2, 3 and 5 and mediates nuclear factor-kappaB activation. Biochem J 2003;371:395–403.
7. Saitoh T, Nakayama M, Nakano H, et al. TWEAK induces NF-kappaB2 p100 processing and long lasting NF-kappaB activation. J Biol Chem 2003;278:36005–36012.
8. Wiley SR, Winkles JA. TWEAK, a member of the TNF superfamily, is a multifunctional cytokine that binds the TweakR/Fn14 receptor. Cytokine Growth Factor Rev 2003;14:241–249.
9. Jakubowski A, Ambrose C, Parr M, et al. TWEAK induces liver progenitor cell proliferation. J Clin Invest 2005;115:2330–2340.
10. Jin L, Nakao A, Nakayama M, et al. Induction of RANTES by TWEAK/Fn14 interaction in human keratinocytes. J Invest Dermatol 2004;122:1175–1179.
11. Michaelson JS, Cho S, Browning B, et al. Tweak induces mammary epithelial branching morphogenesis. Oncogene 2005;24: 2613–2624.
12. Xu H, Okamoto A, Ichikawa J, et al. TWEAK/Fn14 interaction stimulates human bronchial epithelial cells to produce IL-8 and GM-CSF. Biochem Biophys Res Commun 2004;318:422–427.
13. Kawakita T, Shiraki K, Yamanaka Y, et al. Functional expression of TWEAK in human colonic adenocarcinoma cells. Int J Oncol 2005;26:87–93.
14. Nakayama M, Ishidoh K, Kojima Y, et al. Fibroblast growth factor-inducible 14 mediates multiple pathways of TWEAK-induced cell death. J Immunol 2003;170:341–348.
15. Booth D, Haley JD, Bruskin AM, et al. Transforming growth factor-B3 protects murine small intestinal crypt stem cells and animal survival after irradiation, possibly by reducing stem-cell cycling. Int J Cancer 2000;86:53–59.
16. Leedham SJ, Brittan M, McDonald SA, et al. Intestinal stem cells. J Cell Mol Med 2005;9:11–24.
17. Campbell S, Burkly LC, Gao HX, et al. Proinflammatory effects of TWEAK/Fn14 interactions in glomerular mesangial cells. J Immunol 2006;176:1889–1898.
18. Dohi T, Fujihashi K, Kiyono H, et al. Mice deficient in Th1- and Th2-type cytokines develop distinct forms of hapten-induced colitis. Gastroenterology 2000;119:724–733.
19. Dohi T, Fujihashi K, Rennert PD, et al. Hapten-induced colitis is associated with colonic patch hypertrophy and T helper cell 2-type responses. J Exp Med 1999;189:1169–1180.
20. Tran NL, McDonough WS, Savitch BA, et al. Increased fibroblast growth factor-inducible 14 expression levels promote glioma cell invasion via Rac1 and nuclear factor-kappaB and correlate with poor patient outcome. Cancer Res 2006;66:9535–9542.
21. Vidal K, Grosjean I, Evillard JP, et al. Immortalization of mouse intestinal epithelial cells by the SV40-large T gene. Phenotypic and immune characterization of the MODE-K cell line. J Immunol Methods 1993;166:63–73.